JGR Atmospheres

RESEARCH ARTICLE
10.1029/2020JD033653

A Positive Cloud-to-Ground Flash Caused by a Sequence of Bidirectional Leaders that Served to Form a Ground-Reaching Branch of a Pre-Existing Horizontal Channel

Bin Wu[1,2], Weitao Lyu[1,2], Qi Qi[1,2], Ying Ma[1,2], Lyuwen Chen[3], Ruijiao Jiang[1,2,4], Yanan Zhu[5], and Vladimir A. Rakov[4]

[1]State Key Laboratory of Severe Weather, Chinese Academy of Meteorological Sciences, Beijing, China, [2]Laboratory of Lightning Physics and Protection Engineering, Chinese Academy of Meteorological Sciences, Beijing, China, [3]Institute of Tropical and Marine Meteorology, China Meteorological Administration, Guangzhou, China, [4]Department of Electrical and Computer Engineering, University of Florida, Gainesville, FL, USA, [5]Earth System Science Center, University of Alabama in Huntsville, Huntsville, AL, USA

Key Points:

- Bidirectional leaders developed below a previously formed horizontal channel and served to form a new positive branch that attached to the ground
- Connection of the negative (upper) end of each bidirectional leader to the horizontal channel resulted in abrupt elongation of the positive (lower) end
- Flickering streamer-like filaments (needles) extended sideways from the horizontal channel in response to the injection of negative charge associated with the positive cloud-to-ground flash

Supporting Information:

Supporting Information may be found in the online version of this article.

Correspondence to:

W. Lyu,
wtlu@ustc.edu

Citation:

Wu, B., Lyu, W., Qi, Q., Ma, Y., Chen, L., Jiang, R., et al. (2021). A positive cloud-to-ground flash caused by a sequence of bidirectional leaders that served to form a ground-reaching branch of a pre-existing horizontal channel. *Journal of Geophysical Research: Atmospheres*, *126*, e2020JD033653. https://doi.org/10.1029/2020JD033653

Received 4 AUG 2020
Accepted 19 MAY 2021

Abstract High-speed video and electric field change data were used to analyze the initiation and propagation of four predominantly vertical bidirectional leaders making connection to a predominantly horizontal channel previously formed aloft. The four bidirectional leaders sequentially developed along the same path and served to form a positive branch of the horizontal in-cloud channel, which became a downward positive leader producing a 135-kA positive cloud-to-ground (+CG) return stroke. The positive (lower) end of each bidirectional leader elongated abruptly at the time of connection of the negative (upper) end to the pre-existing channel aloft. Thirty-six negative streamer-like filaments (resembling recently reported "needles") extended sideways over ~110 to 740 m from the pre-existing horizontal channel at speeds of ~0.5 to 1.9 × 10^7 m/s, in response to the injection of negative charge associated with the +CG.

Plain Language Summary This paper presents high-speed video records that show how a sequence of predominantly vertical bidirectional leaders can lead to formation of a positive branch of the previously formed predominantly horizontal channel aloft, with this branch eventually making contact with the ground and initiating a positive cloud-to-ground (+CG) return stroke. Additionally, the recently discovered "needles" have been optically imaged and characterized. Observations were performed at the Tall-Object Lightning Observatory in Guangzhou (TOLOG), China. This study helps to improve our understanding of one of the initiation mechanisms of +CG flashes that involves downward branching of in-cloud lightning channels.

1. Introduction

One of the most challenging issues in the physics of lightning is the interpretation of the initiation mechanisms of positive cloud-to-ground (+CG) discharges. According to Rakov and Uman (2003), +CG can be just a byproduct of a cloud discharge. Recently, Nag and Rakov (2012) described six conceptual cloud charge configurations and scenarios that were observed or hypothesized to give rise to positive lightning, with one of the scenarios being a positive branch of an in-cloud discharge channel (see Section 2.6 and Figure 1f in their paper). High-speed video images of such flashes are found in the works of Kong et al. (2008) and Saba et al. (2008, 2009). However, as of today there are no documented cases showing the process of such branch formation. Observations show that branches of in-cloud channels can involve a sequence of bidirectional leaders (Warner et al., 2016; Yuan et al., 2019) that, in effect, can facilitate connection of a channel aloft to ground (Tran and Rakov, 2016).

High-speed video and very high frequency (VHF) observations are two widely used methods to analyze the dynamics of leader initiation and propagation. However, the relatively strong negative breakdown VHF signals associated with the negative end of bidirectional leaders, tend to mask the relatively weak positive breakdown VHF signals associated with the simultaneously propagating positive end (Shao et al., 1999). Consequently, it is often difficult for VHF imaging systems to detect the positive end of bidirectional leaders. Bidirectional propagation of leaders can be detected (imaged) with high-speed video cameras that have

yielded important results published by Jiang et al. (2014), Kostinskiy et al. (2015), Montanyà et al. (2015), Takamatsu et al. (2015), Tran and Rakov (2016), Yuan et al. (2019), Warner et al. (2016), and Wu, Lyu, Qi, Ma, Chen, Jiang et al. (2019). In particular, Montanyà et al. (2015) reported a recording of bidirectional intracloud lightning initiation in virgin air at ~11,000 frames per second (fps). Tran and Rakov (2016) observed that the negative end of a bidirectional leader contacted ground and produce a negative cloud-to-ground return stroke (RS). However, bidirectional leaders often develop completely inside the cloud, which makes their optical imaging difficult. Only a few quality recordings are presently available. As a result, the details of dynamics of bidirectional leaders resulting in the formation of a ground-reaching leader are still not completely understood.

Positive lightning discharges account for about 10% of all CG discharges (e.g., Rakov, 2003), so positive lightning discharges are considerably less studied and understood than their negative counterparts. Furthermore, most of the existing optical observations of +CG flashes can only yield some characteristics after the leader emerges from the cloud. To the best of our knowledge, to date, there are no optical records of the complete dynamics of +CG flashes. High-speed video observations reviewed above confirm that in-cloud channels giving rise to CG discharges can be produced by bidirectional leaders. However, details of the formation of a downward positively charged ground-reaching branch have not been reported before.

In this paper, we present optical and electric field observations of the formation process of ground-reaching positive branch of an in-cloud channel initiating a +CG RS. The observations were performed at the Tall-Object Lightning Observatory in Guangzhou (TOLOG), China. The dynamics of all stages of the +CG flash are examined and discussed in detail. Among other things, our records show flickering streamer-like filaments (resembling recently reported "needles" observed with radiofrequency (RF) imaging systems by Hare et al. (2019) and Pu and Cummer. (2019) and optically by Saba et al. (2020)) extending sideways from the horizontal in-cloud channel energized by the +CG.

2. Instrumentation and Data

The TOLOG (Lu et al., 2012, 2013; Qi et al., 2018; Wu, Lyu, Qi, Ma, Chen, Zhang et al., 2019) is located on the roof of an approximately 100-m-high building of the Guangdong Meteorological Bureau. The optical instrumentation used in this study consisted of a lightning channel imager (LCI) and two high-speed video cameras (HC-1 and HC-2) operating at different framing rates (20,000-fps and 50,000-fps, respectively). The focal lengths of HC-1 and HC-2 were 14 and 20 mm, respectively, and the record lengths were 50 and 20 ms, respectively. The corresponding pre-trigger times were 25, and 10 ms and the corresponding spatial resolutions were 1,024 pixels × 1,024 pixels and 512 pixels × 272 pixels. The framing rate and focal length of the LCI were 50-fps and 5 mm, respectively. The record length, corresponding pre-trigger time and corresponding spatial resolution of LCI were 2 s, 500 ms, and 780 pixels × 582 pixels, respectively.

Electric field changes were measured using a set of fast and slow antenna systems. The time constants of the fast and slow antennas were 1 ms and 6 s, respectively, and the sampling rate of the two field measuring systems was 10 MHz. The record lengths and pre-trigger times of the fast and slow antenna systems were 1 s and 100 ms, respectively. The measurement ranges of the fast and slow antenna systems were ±100 kV/m and ±200 kV/m, respectively, and the vertical resolution of each of them was 12-bit.

Signals from one of the eight channels of the Lightning Attachment Process Observation System (Wang et al., 2011) recorded by a digital oscilloscope was used for triggering the cameras and the field measuring systems. Each trigger event was time-stamped using a GPS clock with accuracy of 30 ns. In addition, we obtained information on the location of lightning channel ground termination point, the time of RS, and the estimated peak current of the +CG RS from the Guangdong-Hong Kong-Macao Lightning Location System (GHMLLS).

The +CG flash (denoted F17149) considered here contained a single stroke. The GHMLLS reported that stroke to be located approximately 17 km from the observation station and estimated its peak current to be approximately +135 kA. In this paper, we analyzed the characteristics of bidirectional leaders involved in the initiation and development of the +CG. Additionally, we examined streamer-like filaments extending sideways from the horizontal in-cloud channel energized by the +CG. All the lengths and speeds presented

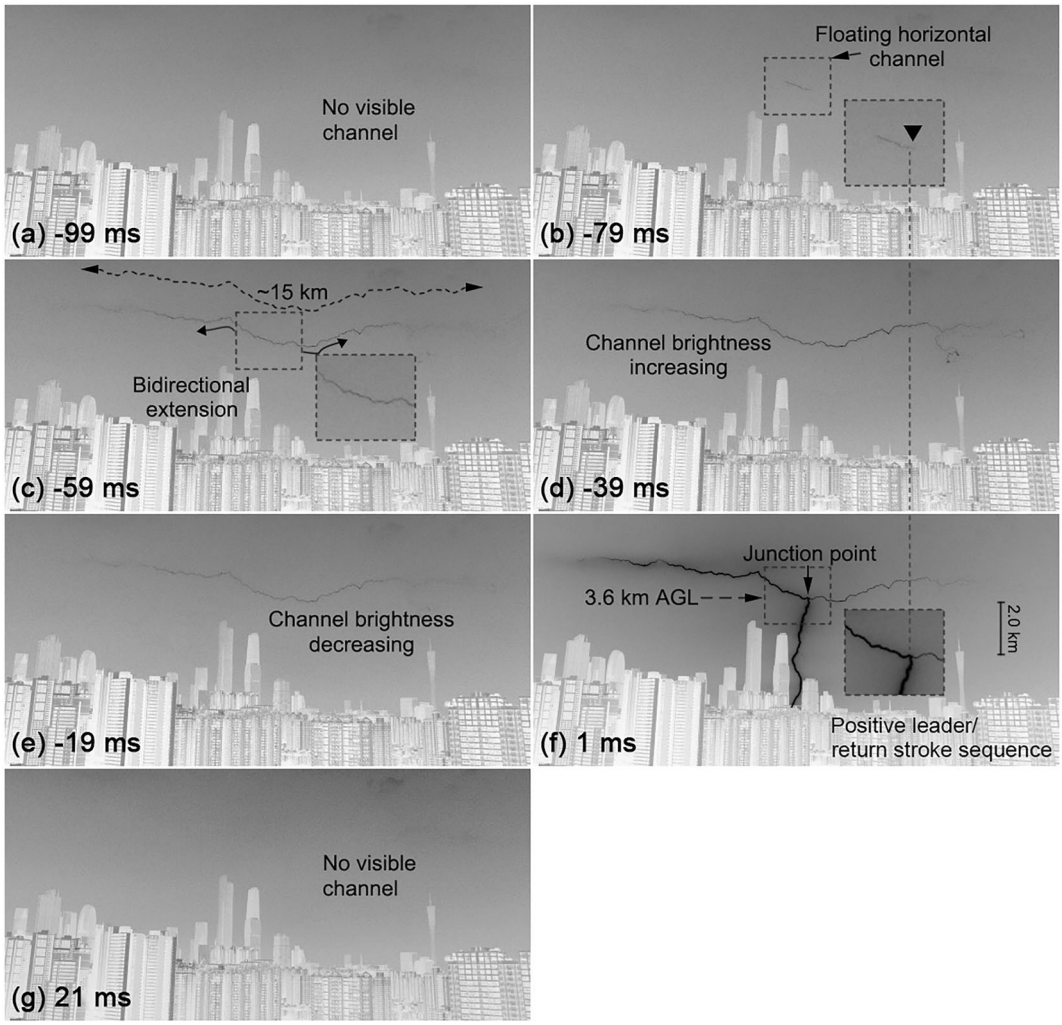

Figure 1. Seven consecutive images obtained using the lightning channel imager operating at 50 frames per second (20-ms interframe interval). The time stamp on each image corresponds to the end of exposure time, adjusted based on synchronized images from high-speed video camera (HC-1). The images were cropped, inverted, and contrast enhanced. Portions of images in smaller broken-line boxes are shown enlarged in (b), (c), and (f). Small inverted triangle in (b) indicates the inferred origination point of the predominantly horizontal channel, whose development is seen in (b) and (c).

are two-dimensional (2-D) and estimated based on the distance between the +CG ground termination point and TOLOG. All times are relative to the onset of the RS of the +CG flash. The atmospheric electricity sign convention was used in this study.

3. Data Presentation and Results

The LCI operated at 50-fps (20-ms interframe interval) with a recording time of 2 s and completely recorded the entire +CG lightning flash (see Movie S1 in the supporting information). Figure 1 shows seven consecutive LCI images, with an exposure time of approximately 20 ms each, with the time stamp on each image being the end of exposure time relative to the return-stroke onset. No luminous channels were seen for about 500 ms in the LCI record prior to the −79-ms frame. A short floating channel appeared in the −79-ms frame (see the smaller rectangular box and its expansion in Figure 1b). The floating channel became visible during the −99 to −79 ms time interval and then clearly exhibited bidirectional development extending horizontally over about 15 km from −79 to −59 ms (see Figure 1c).

In the next two frames (see Figures 1d and 1e), the bidirectional leader channel did not exhibit further extension, but its brightness increased from −59 to −39 ms and then decreased from −39 to −19 ms. The predominantly vertical (positive leader/RS sequence) channel connecting the previously formed predominantly horizontal channel with the ground is seen in Figure 1f. However, due to the insufficient temporal resolution of LCI, the dynamics of that connection is not resolved in Figure 1. Note that the junction point between the positive leader/RS channel and the previously formed horizontal channel was near the right end of the initial horizontal channel segment seen in Figure 1b (see vertical broken line passing through Figures 1b, 1d, and 1f).

We now present our records obtained using the high-speed video camera (HC-1) operating at 20,000-fps (50-μs interframe interval) with a recording time of 50 ms. These records (see Movie S2 in the supporting information) clearly show that the downward positive leader evolved from a sequence of four bidirectional leaders that developed along the same, predominantly vertical path below the predominantly horizontal channel whose development is seen in Figure 1. Figure 2a shows a composite image of 40 selected HC-1 frames before the onset of the +CG RS. These frames were selected to best display the geometry of the horizontal channel aloft and the following four bidirectional leaders, the last of which completed the formation of the downward branch of the horizontal channel, which forged its way to ground and produced the +CG RS.

Figure 2b shows the image brightness record along with the fast and slow antenna system electric field changes. The bipolar pulses (labeled BPs) in the fast electric field change record (labeled fast antenna (FA) in Figure 2b) that occurred about 60 ms prior to the return stroke (labeled +RS) corresponds to the full (about 15 km) extension of the horizontal channel seen in Figure 1c (−59-ms, end of exposure time). Between −50 and −40 ms, K change type signatures are seen in the fast electric field change record. Note that between −59 and −39 ms, the brightness of the horizontal channel increased (see Figure 1d). It follows from Figure 1 that no vertical channel was formed before −19 ms. However, at that time the slow electric field change record, labeled slow antenna (SA) in Figure 2, shows significant positive (opposite to the +RS) field deflection, which is indicative of the motion of positive charge toward the observer. In fact, the positive field deflection started at about −60 ms, and the slow field change between −60 ms and 0 is characteristic of downward positive leader signature, although the downward extension apparently did not start until −19 ms or so. It is likely that the positive charge motion toward the observation station between −60 and −19 ms is indicative of the entire horizontal channel being charged positively. Electric field signatures of the beginning and the intensification of this latter process in the FA record are marked as "BPs" and "K changes," respectively, in Figure 2b.

Four bidirectional leaders (BL_1–BL_4) associated with formation of downward positive leader occurred approximately 20, 12, 9, and 4 ms before the onset of the +CG RS (see the brightness trace in Figure 2b). BL_1 to BL_4 produced no pronounced electric field changes (see the FA and SA traces in Figure 2b), because they were relatively far (approximately 17 km) from observation station. The upper end of each bidirectional leader extended upward (this extension is imaged for BL_1, BL_3, and BL_4 and inferred for BL_2) and contacted the previously formed horizontal channel, forming a downward branch of the horizontal channel that eventually made contact with the ground. The height of the junction point was approximately 3.6 km above ground level (AGL). The polarity of charge transfer to ground was positive, based on the negative electric field change at $t = 0$ (see +RS in Figure 2b). Consequently, the lower end of each bidirectional leader must have been positive, with the upper end being negative and the horizontal channel aloft (at least near the junction point) being positive.

During the +CG RS stage, the left part of the horizontal channel was much brighter than the right one (see Movies S2 and S3 in the supporting information), which suggests that positive charge was supplied to the vertical channel to ground mostly by the left part of the horizontal channel. However, the brightness of the right part also increased during the return-stroke stage and, hence, it also participated in delivering positive charge to the junction point (in other words, the negative charge injected by the +CG RS into the junction point moved both to the left and to the right along the horizontal channel). Further, during BL_1–BL_4 (approximately −20 ms to 0), the electric field was dominated by the motion of positive charge toward the observation station (see the SA trace in Figure 2b), which indicates that the middle part of the floating horizontal channel (near the prospective junction point) was positive. There were other bidirectional leaders

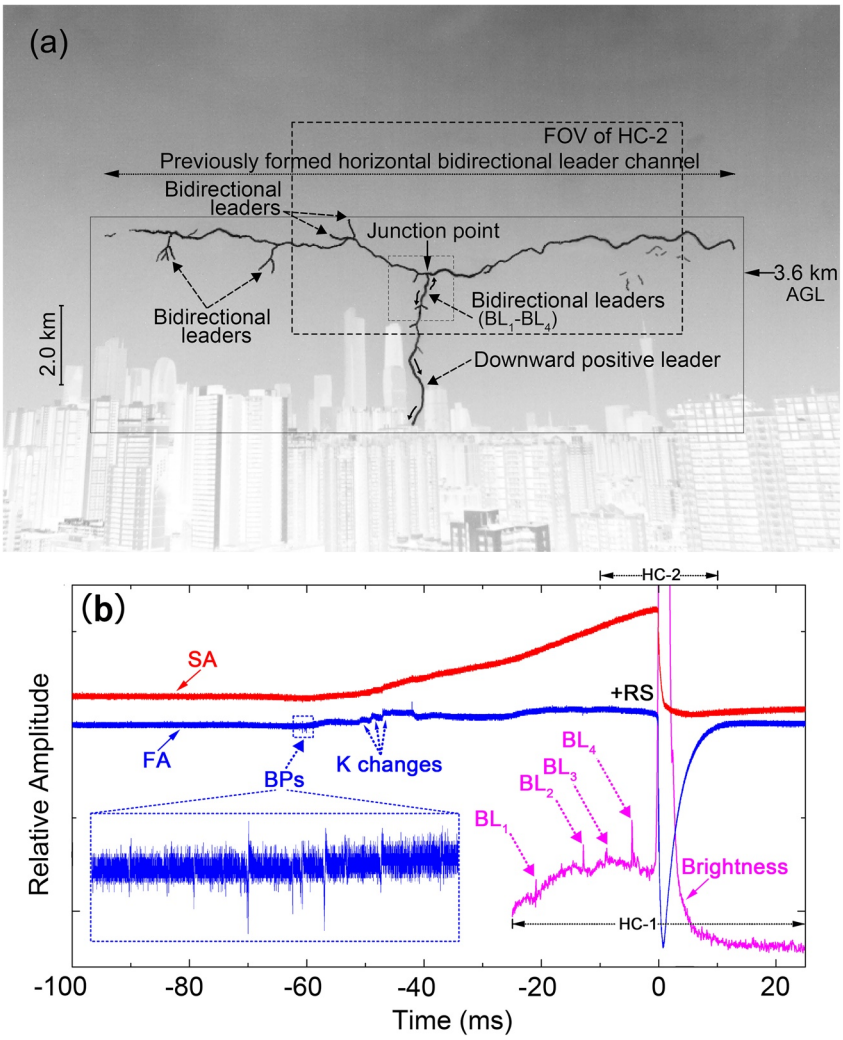

Figure 2. (a) Composite image of 40 selected frames (from −25 to −0.05 ms) obtained using high-speed video camera (HC-1) operating at 20,000 frames per second (50-μs interframe interval), showing the geometry of downward positive leader channel to ground (formed via a sequence of four bidirectional leaders, which connected to the previously formed horizontal channel aloft). (b) Synchronized optical image brightness (the sum of gray values of all pixels in each HC-1 image) within −25 to 25 ms time window, and fast (FA) and slow (SA) electric field change records (from −100 to 25 ms). The image shown in (a) was cropped, inverted, and contrast enhanced. The curved arrows indicate the observed directions of channel extension. Single-frame and composite HC-1 images of the solid-line rectangular area seen in (a) that show the salient features of the discharge development after the formation of the horizontal channel aloft are presented in Figures 3a–3n. The dashed-line rectangular box in (a) shows the field of view of HC-2. The time window corresponding to images recorded by HC-2 is from −10 to 10 ms. The larger dashed-line rectangular box in (b) is an expanded view for the smaller dashed-line rectangular box labeled BPs. Labels BL_1–BL_4 are used to mark four bidirectional leaders examined in detail. AGL, above ground level; BPs, bipolar pulses; FA, fast antenna; +RS, positive return stroke; SA, slow antenna.

that served to form short branches in the left part of the horizontal channel (see Bidirectional leaders appeared on the left part of the horizontal channel in Figure 2a). Those are not further discussed in this paper.

Figure 3 shows key processes seen in the HC-1 records inside the solid-line rectangular box in Figure 2a after the formation of horizontal channel aloft. Four bidirectional leaders (BL_1–BL_4) sequentially initiated and developed along the same predominantly vertical path below the previously formed horizontal channel. The positive (lower) end of each following bidirectional leader was closer to the ground than that of the preceding one (see Figures 3b, 3d, 3f, and 3h). The lengths of four bidirectional leaders (BL_1–BL_4) progressively increased by approximately 190 m from BL_1 to BL_2, 250 m from BL_2 to BL_3, and 370 m from BL_3 to BL_4.

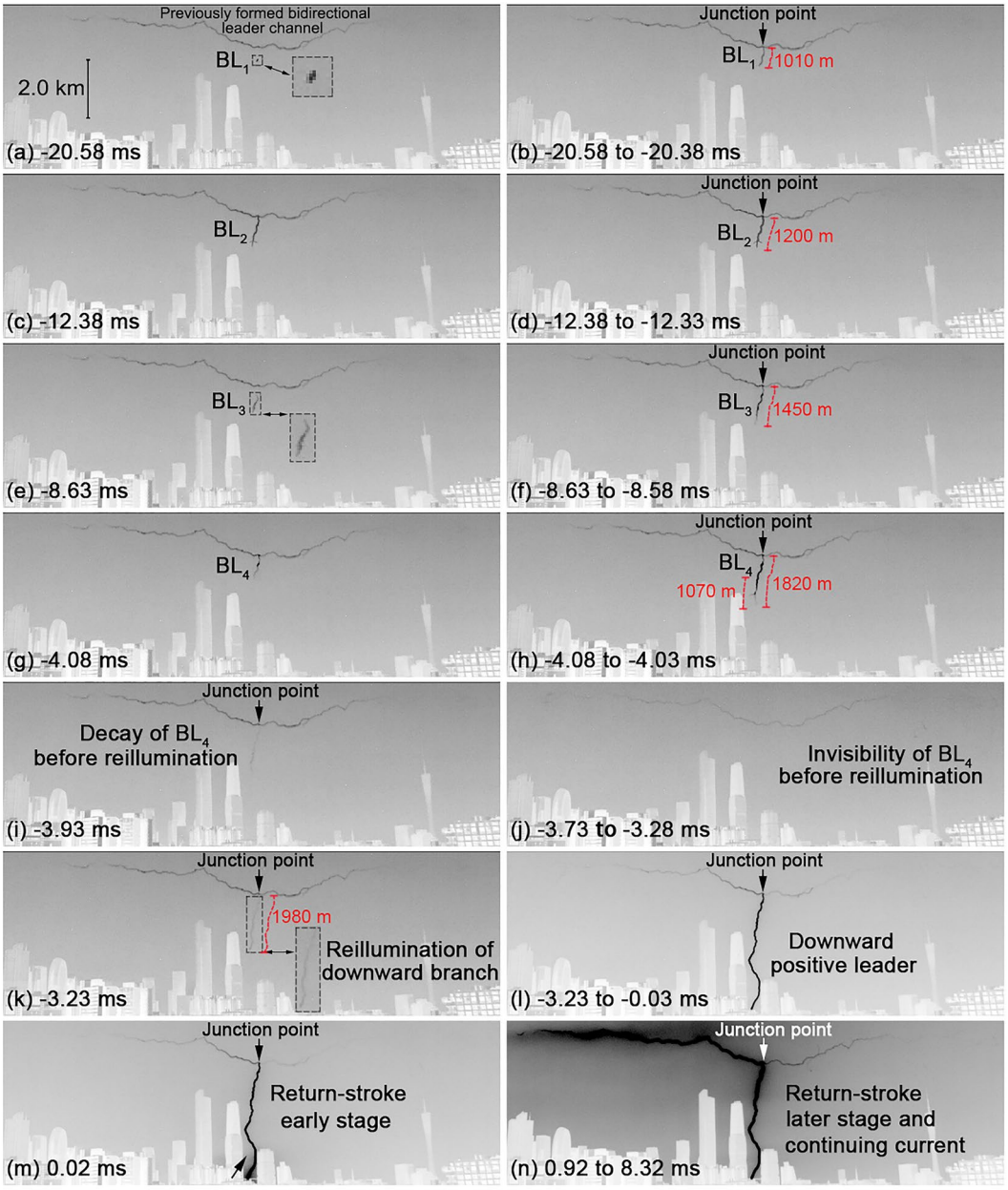

Figure 3. Key processes seen in high-speed video camera (HC-1) (50-μs interframe interval) records inside the solid-line rectangular box shown in Figure 2a after the formation of horizontal channel aloft: (a) First image of the first bidirectional leader (BL_1) channel, (b) composite image showing maximum extent of the BL_1 channel, (c) first image of the second bidirectional leader (BL_2) channel, (d) composite image showing maximum extent of the BL_2 channel, (e) first image of the third bidirectional leader (BL_3) channel, (f) composite image showing maximum extent of the BL_3 channel, (g) first image of the fourth bidirectional leader (BL_4) channel, (h) composite image showing maximum extent of the BL_4 channel, (i) image of decaying fourth bidirectional leader (BL_4) channel (downward branch), (j) image in which the downward branch is undetectable, (k) first image showing reillumination of the downward branch formed via the sequence of BL_1 to BL_4, (l) composite image showing the fully formed downward positive leader, (m) image of the return-stroke early stage, (n) composite image showing the return-stroke later stage and continuing current. Time labels correspond to the end of frame exposure times measured with respect to the return stroke onset. Red dashed lines are used to show the lengths of channel segments of BL_1–BL_4 and of the resultant downward branch. Images from 0.02 to 0.92 ms are overexposed.

The sequence of four bidirectional leaders (BL_1–BL_4) served to form a new downward positive branch of the horizontal channel. The newly formed downward branch gradually decayed within ~0.3 ms (see Figures 3h and 3i) and became undetectable (see Figure 3j). Then this branch reilluminated (see Figure 3k) and continued extending toward ground. Comparing the positions of its tip in Figures 3h and 3k, we found that the downward branch elongated by ~160 m, while its luminosity was undetectable for ~0.45 ms (see Figure 3j).

Then the re-illuminated downward branch evolved into a fully developed downward positive leader (see Figure 3l), attached to the ground, and initiated a +CG RS (see Figure 3m). Based on (not shown here) consecutive frames of HC-1 and HC-2 (obtained from Movies S2 and S3 in the supporting information), the entire discharge channel (including the vertical channel to ground and both left and right parts of the horizontal channel) exhibited light blooming during the +CG RS, but the brightness increase of the left part of the horizontal channel was significantly larger than that of the right part. During the later stage of RS and continuing current, the left part maintained elevated brightness, while the right part just returned to the brightness level seen before the RS (see Figure 3n). Therefore, as noted earlier, it appears that mostly the left part was active during the positive leader/RS sequence, although the right part also contributed some current, particularly during the continuing current stage, as seen in Figure 7.

Figures 4a–4h show eight consecutive images of BL_1, and six consecutive images of BL_2 are shown in Figures 4i–4n. BL_1 initiated at a height of 3.1 km AGL and at a distance of ~500 m from the horizontal channel above it. Its bidirectional extension is clearly seen in Figures 4b and 4c, although its lower end became undetectable in Figure 4d. By overlaying the BL_1 channels in Figures 4c and 4d, we found that the two channels had a common part. It is possible that the lower part of the BL_1 channel in Figure 4d decayed, while its upper part survived and eventually made connection to the horizontal channel as seen in Figure 4e.

After the connection, the luminosity of BL_1 and the left part of the horizontal channel increased significantly, while the luminosity of its right part diminished (see Figure 4f). The connection was also associated with elongation of BL_1 channel by approximately 530 m (see Figure 4f), retracing the previously formed but decayed BL_1 channel seen in Figure 4c. The effective 2-D elongation speed was approximately 1.1×10^7 m/s. Then the new positive branch formed by BL_1 gradually decayed (see Figure 4g) and became undetectable in Figure 4h.

It is unknown whether the polarity reversal (neutral) point of BL_1 was stationary at 3.1 km AGL (see Figure 4b) or moved up as its lower part decayed (see Figure 4d). In the former case, the extension of the negative end was approximately 500 m (see Figure 4f), which is about the same as the extension of the positive end (approximately 510 m). In the latter case, the extension of the negative end was approximately 300 m (see Figure 4f), with the positive end extension being approximately 710 m.

Figure 4i shows the frame just preceding the occurrence of BL_2 (7.85 ms after the decay of BL_1). In its first image (Figure 2j), BL_2 appears to be already connected to the horizontal channel aloft, which can be due to insufficient temporal resolution of the camera or low (undetectable) brightness of BL_2 channel in Figure 4i. BL_2 followed the decayed channel of BL_1 (compare Figures 4j and 4f). Further, the brightness of the new branch formed by BL_2 and the left part of the horizontal channel in Figure 4k increased, similar to Figure 4f. This similarity makes us believe that event BL_2 was indeed a bidirectional leader. Note branching at the lower (positive) end of the BL_2 channel (see Figures 4j and 4k), which is usually considered as evidence of leader extension in virgin air (e.g., Tran and Rakov, 2016).

Unlike BL_1 and BL_2, BL_3 and BL_4 were recorded, with a better time resolution (20-μs interframe interval), by HC-2 (see Movie S3 in the supporting information), within −10 to 10 ms time windows shown in Figure 2b. The dynamics of BL_3 and BL_4 are shown in Figure 5. Figures 5a–5f show six consecutive images of BL_3, which occurred approximately 3.5 ms after BL_2. The initiation height of BL_3 (2.9 km AGL and 700 m below the horizontal channel) was approximately 200 m lower than that of BL_1. BL_3 initiated and extended bidirectionally in the remnants of the decayed channel of BL_2. Similar to BL_1, brightness of the left part of the horizontal channel and that of BL_3 itself increased after the connection of the negative (upper) end of BL_3 to the horizontal channel (see Figures 5e and 4f). However, in contrast to BL_1, BL_3 was extending without interruption until its connection to the horizontal channel (see Figures 5c–5e).

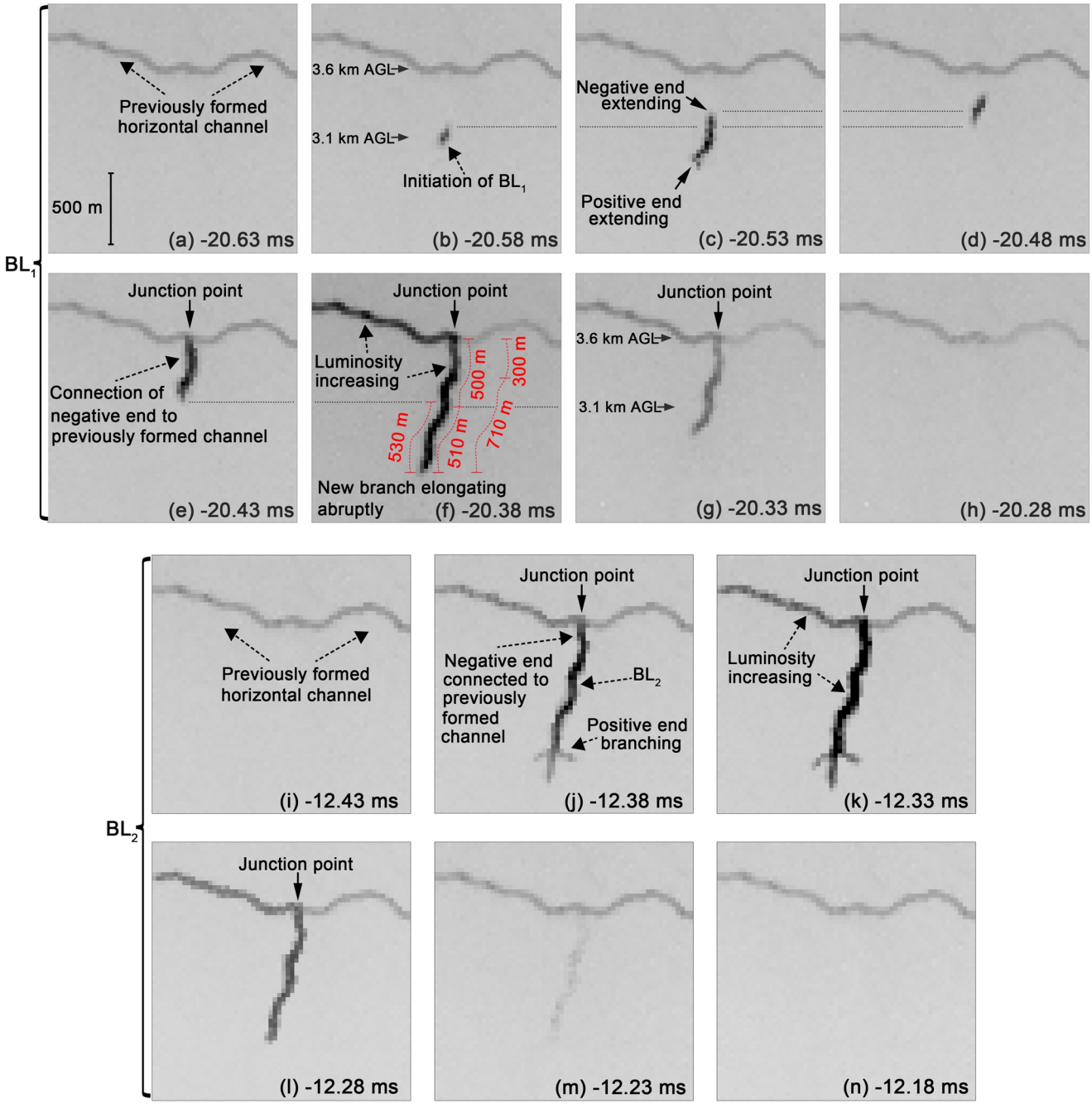

Figure 4. (a–h) Eight consecutive high-speed video camera (HC-1) (50-μs interframe interval) images of the evolution of first bidirectional leader (BL_1) and (i–n) six consecutive HC-1 images of the second bidirectional leader (BL_2) within the small dotted-line rectangular box shown in Figure 2a. The solid-line rectangular box labeled 3 in panel (d) is a superposition of boxes labeled 1 and 2 in panels (c) and (d), respectively. Each image was inverted and contrast enhanced. The time stamp given on each image is the end of the exposure time. Red dashed lines are used to show the lengths of negative and positive ends of BL_1. For BL_2, no upward extension was detected, probably due to insufficient time resolution of the camera or low (undetectable) brightness of BL_2 channel in (i). AGL, above ground level; BL, bidirectional leader.

In Figure 5e, the positive (lower) end of BL_3 extended by approximately 380 m relative to its position in Figure 5d. It is unknown whether this extension occurred before or after the negative (upper) end of BL_3 connected to the horizontal channel aloft. No further extension is seen in Figure 5f. The overall length of the negative end of BL_3 was approximately 730 m (see Figure 5f), which is almost the same as that of the positive end (approximately 720 m).

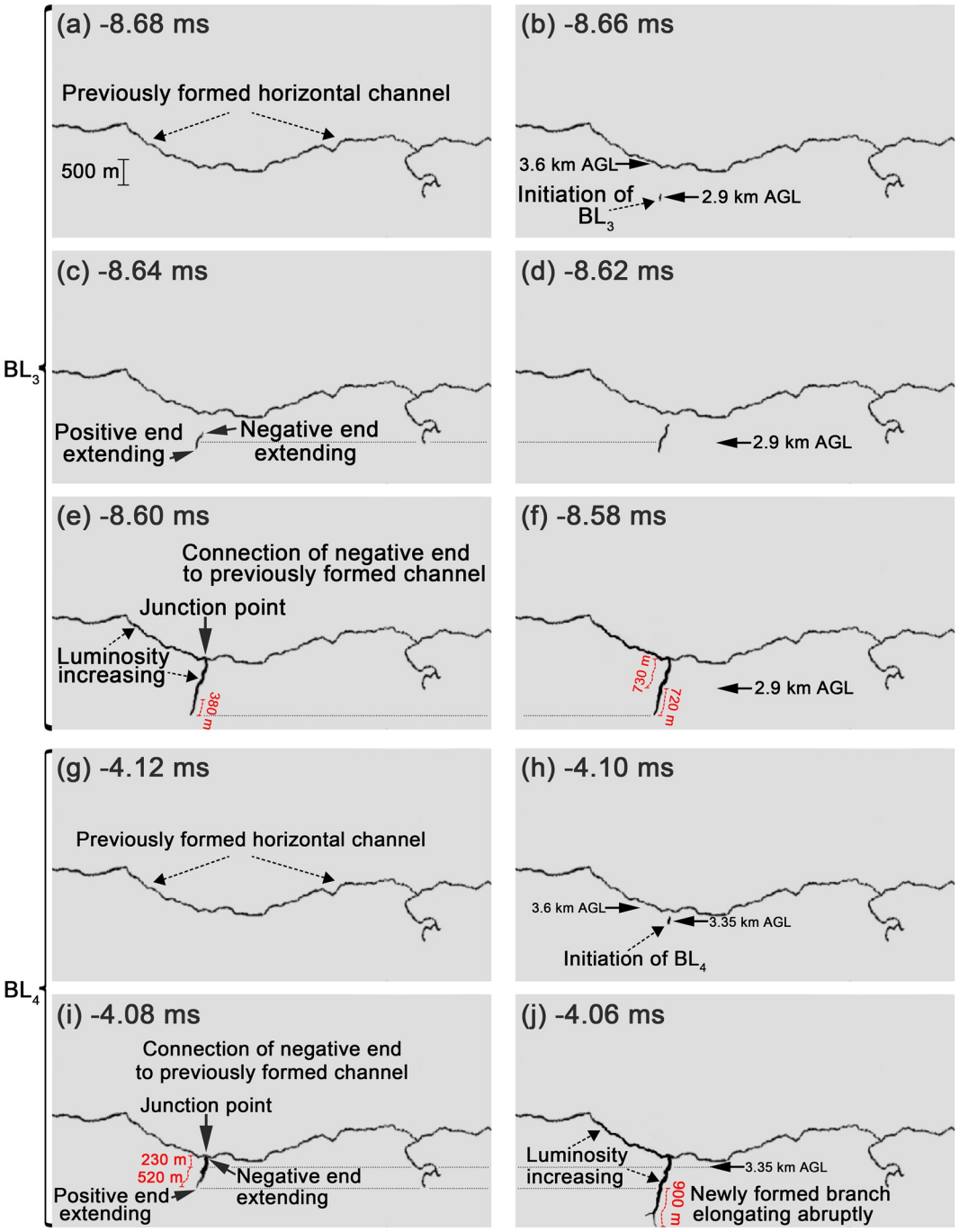

Figure 5. (a–f) Six consecutive high-speed video camera (HC-2, 20-μs interframe interval) images of BL_3 and (g–j) four consecutive HC-2 images of BL_4. The images were background removed, inverted, and contrast enhanced. The time stamp given on each image is the end of the exposure time. The dashed-line rectangular box in Figure 2a shows the field of view of HC-2. Red dashed lines are used to show the lengths of channel segments of BL_3 and BL_4. AGL, above ground level; BL, bidirectional leader.

Figures 5g–5j show four consecutive images of BL_4, which occurred approximately 4.5 ms after BL_3. The initial height of BL_4 (3.35 km AGL and 250 m below the horizontal channel) was higher than those of BL_1 and BL_3. BL_4 extended bidirectionally along the decayed channel of BL_3 (see Figures 5h and 5i), and within approximately 20 μs the negative end of BL_4 connected to the horizontal channel (see Figure 5i). The brightness of BL_4 and the left part of the horizontal channel (to the left of the junction point) increased.

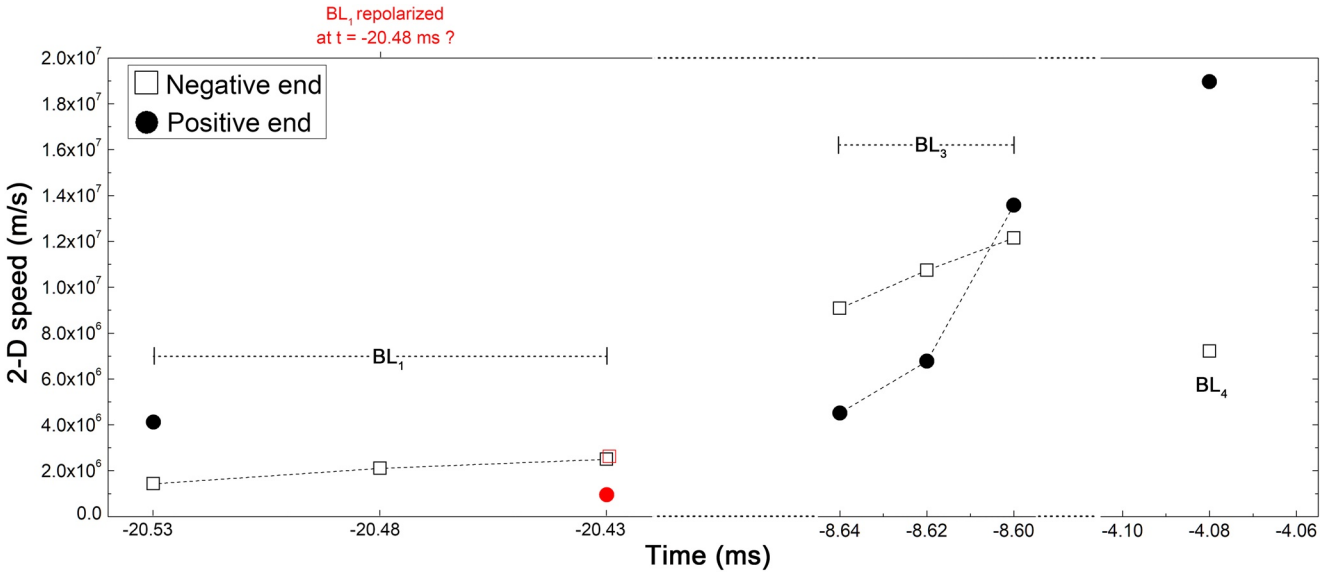

Figure 6. The 2-D speeds of negative and positive ends of the first bidirectional leader (BL_1), the third bidirectional leader (BL_3), and the fourth bidirectional leader (BL_4), based on the consecutive frames shown in Figure 4 (BL_1, HC-1) and Figure 5 (BL_3 and BL_4, HC-2). The red box and red circle at $t = -20.43$ ms represent the speeds of negative and positive ends, respectively, for the case if BL_1 was repolarized.

Due to the positive end of BL_4 extending beyond the lower edge of Figure 5j, we couldn't obtain the total length of the positive end of BL_4 from Figure 5j. According to Figure 3h, the overall length of BL_4 channel was approximately 1,820 m. The total length of the negative (upper) end of BL_4 was approximately 230 m (see Figure 5i), which is considerably shorter than that of its positive (lower) end (approximately 1,590 m).

Like BL_1, BL_4 elongated abruptly (beyond the lower edge of Figure 5i) at the time of its connection to the horizontal channel (see Figures 5i and 5j). The abrupt elongation was by approximately 1,070 m, as seen in Figure 3h, with a 2-D speed of approximately 5.4×10^7 m/s. Note that, similar to BL_2, the lower (positive) end of BL_4 channel was branched (see Figure 5j), which indicates that it extended into virgin air.

We estimated 2-D speeds of the positive and negative ends of BL_1, BL_3 and BL_4, based on the consecutive frames of HC-1 and HC-2 (Figures 4a–4h, 5a–5f, and 5g–5j). Speed profiles for the three bidirectional leaders (BL_1, BL_3, and BL_4) are shown in Figure 6. The 2-D nonzero speeds of the negative and positive ends ranged from 1.4×10^6 to 1.2×10^7 m/s and from 9.5×10^5 to 1.9×10^7 m/s, respectively. The average (mean) speeds of the negative and positive ends were approximately 6.5×10^6 m/s and 8.2×10^6 m/s, respectively. Note that the speeds for the first leader (BL_1) are considerably lower than those for the subsequent leaders (BL_3 and BL_4). The average (mean) extension speed of BL-formed downward branches after the negative BL end connected to the horizontal channel was approximately 3.2×10^7 m/s.

We now present transient streamer-like discharges from the lateral surface of the horizontal channel during the return-stroke later stage and the following continuing current. Figure 7 shows a composite image of 480 selected HC-2 (20-μs interframe interval) frames for the time interval of 0.4 to 10 ms (all after the +CG return-stroke onset). One can see 36 side branches, labeled 1 through 36, extending primarily up and down (radially) from the horizontal channel when the negative charge associated with the return-stroke later stage and the following continuing current was injected into the horizontal channel core, probably surrounded by a positive space charge sheath. These branches are numbered in the order of their occurrence relative to the RS onset. Their time of occurrence is color coded. Because these transient events were relatively far from the observation station, they produced no detectable electric field changes (see FA and SA traces in Figure 2b). These branches appear to be streamer filaments originating from the lateral surface of the horizontal channel, since they are noticeably fainter and thinner than their parent channel.

These side branches were transient; that is, they decayed soon after extending from the horizontal channel. Then some of the decayed (non-luminous) side branches were reilluminated by one or more recoil leader

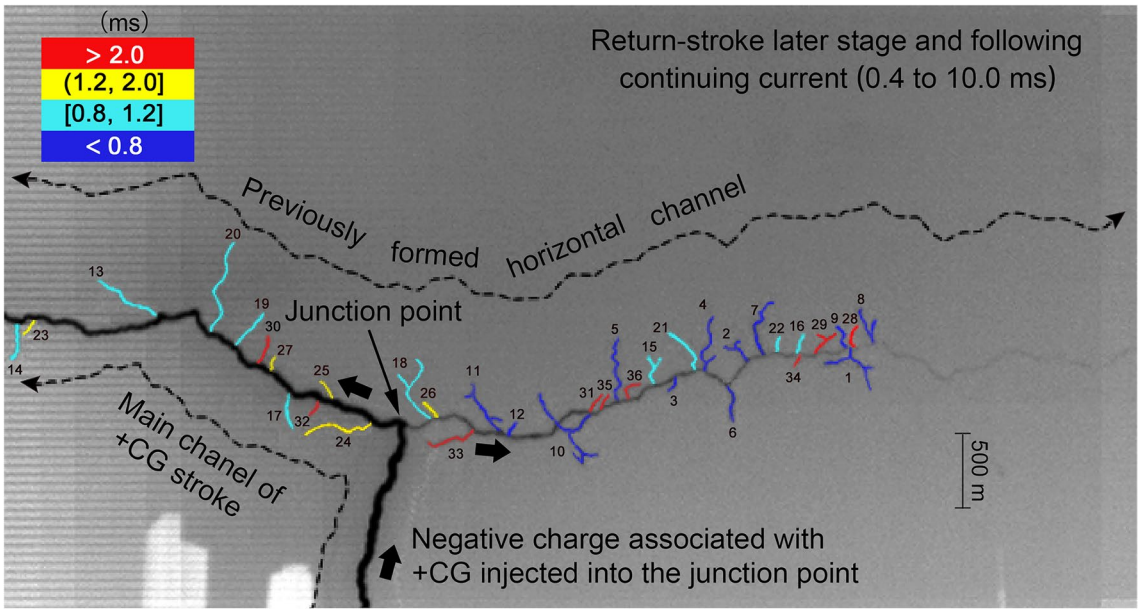

Figure 7. Composite image of 480 selected frames (from 0.4 to 10.0 ms) obtained using high-speed video camera (HC-2, 20-μs interframe interval) showing side branches (different colors indicate their occurrence time relative to the return stroke (RS) onset) originating from the horizontal channel during the return-stroke later stage and continuing current. The composite image was inverted and contrast enhanced. Thick arrows indicate the direction of motion of negative charge associated with the +CG RS and continuing current along the vertical and horizontal channels. Discernible side branches (streamer-like filaments) are numbered 1 to 36 in the order of their occurrence relative to the RS onset.

or streamer type events. At the same time, some new side branches were extending from other parts of the horizontal channel. Therefore, the branches seen in Figure 7 are the cumulative effect of their formation process and reillumination by the recoil type processes. Note that the recoil events caused the flickering of side branches.

Characteristics of the 36 streamer-like filaments including time intervals relative to the preceding one, 2-D lengths, and 2D extension speeds, are given in Table 1. We calculated the time interval between consecutive side branches as the interval between the time corresponding to the first image of a given side branch and that of the preceding one. It is unknown whether the channel seen in the first frame (0.40 ms) of #1 is true first image or one of its subsequent flickerings, due to the overexposure of the images caused by the +CG RS. For this reason, we do not give the initiation time and 2-D extension speed of #1 in Table 1. The side (more or less radial) branches were observed within 0.4–10 ms of the onset of +CG RS and extended away from the horizontal channel over approximately 110 to 740 m (mean = 290 m) at speeds of approximately 5.0–19 × 10^6 m/s (mean = 9.6 × 10^6 m/s). The time intervals between the side branches ranged from 0 to 2.32 ms (mean = 250 μs).

It is unknown whether similar streamer-like filaments occurred before 0.4 ms due to overexposure of the images caused by the +CG RS. Before 0.8 ms, streamer-like filaments appeared only on the right part of the horizontal channel. From 0.8 to 1.2 ms, streamer-like filaments appeared on both the left and right parts of the horizontal channel. From 1.2 to 2.0 ms, streamer-like filaments, except for #26 appeared only on the left part of the horizontal channel. After 2.0 ms, streamer-like filaments, except for #30 and #32 appeared only on the right part of the horizontal channel. No new streamer-like filaments were identified after 9.0 ms (see the second column in Table 1).

Note that both the left and the right parts of the horizontal channel increased in brightness at the RS onset, even though the left part was always brighter. This suggests that both the left and the right parts of the horizontal channel contributed to supplying positive charge to the junction point (or, equivalently, the negative charge injected by +CG into the junction point moved both to the left and to the right along the horizontal channel). The hot (luminous) core of the horizontal channel was probably surrounded by a non-luminous positive space charge sheath, formed during the +CG leader stage. Negative charges pumped into the

Table 1
Characteristics of 36 Flickering Side Branches Shown in Figure 7

Side branch ID	Initiation time relative to RS onset (ms)	Initiation time relative to the preceding side branch (μs)	2-D length (m)	2-D extension speeds (10^6 m/s)
1		–	270	–
2	0.5	–	230	11.5
3	0.52	20	140	7.0
4	0.52	0	420	10.5
5	0.54	20	530	13.3
6	0.56	20	300	15.0
7	0.58	20	500	12.5
8	0.58	0	280	7.0
9	0.62	40	200	10.0
10	0.64	20	580	14.5
11	0.68	40	390	9.8
12	0.7	20	120	6.0
13	0.8	100	530	13.3
14	0.84	40	270	13.5
15	0.84	0	230	11.5
16	0.84	0	150	7.5
17	0.86	20	270	13.5
18	0.9	40	560	14.0
19	0.9	0	320	8.0
20	0.92	20	740	18.5
21	0.96	40	370	9.3
22	1.2	240	120	6.0
23	1.24	40	130	6.5
24	1.34	100	550	13.8
25	1.88	540	170	8.5
26	2	120	150	7.5
27	2	0	110	5.5
28	2.4	400	200	5.0
29	4.72	2,320	220	5.5
30	5.56	840	220	5.5
31	5.98	420	160	8.0
32	6.1	120	130	6.5
33	6.54	440	390	9.8
34	6.6	60	120	6.0
35	7.44	840	140	7.0
36	9	1,560	190	9.5
Mean	–	250	290	9.6

Abbreviation: RS, return stroke.

horizontal channel by the +CG RS and continuing current were probably the cause of side branches (negative breakdowns) developing into and beyond the positive space charge sheath.

Distributions of time intervals between the 36 side branches and their 2-D extension speeds are shown in Figure 8. Minimum and maximum time intervals are 0 and 2.32 ms, respectively, with a mean value of 250 μs. Most of the intervals (~62%) are shorter than 100 μs and ~85% are shorter than 300 μs. In many cases multiple events occurred simultaneously or almost simultaneously (see the second column in Table 1). The minimum and maximum extension speeds are 5×10^6 and 18.5×10^6 m/s, respectively, with a mean value of 9.6×10^6 m/s. In most (60%) of cases, the speed is lower than 10^7 m/s.

4. Discussion and Summary

A sequence of four bidirectional leaders (BL_1-BL_4) served to form a new positive branch originating from the previously formed horizontal channel aloft and eventually attached to the ground and initiated a 135-kA +CG RS. To the best of our knowledge, this is the most detailed study of the process of formation of in-cloud channel branch that extended toward ground and caused +CG to date. Additionally, we observed negative streamer-like filaments extending sideways from the positively charged horizontal channel in response to the injection of negative charge associated with the +CG.

4.1. On a Possible Background Discharge Prior to BL1

Our optical records (including LCI images and high-speed video camera images) show that there were no positive leader or streamer-like branches emanating from the predominantly horizontal channel before BL_1, probably due to (a) not long enough recording time (−25 to 25 ms) of high-speed cameras operating at 20, 000 frames per second, (b) insufficient temporal resolution (~20 ms) of LCI having a longer recording time (2 s), or (c) very low brightness of positive leader or streamer branches within the visible wavelength range (380 to 780 nm) of our cameras.

The 2-D extension speeds of negative and positive ends of BL_1 ranged from 9.5×10^5 to 4×10^6 m/s (see Figure 6), which is near the upper bound or higher than the average extension speed of leaders in virgin air (~10^4 to 10^6 m/s). Such relatively higher extension speeds at the positive and negative ends of BL_1 seem to suggest that BL_1 may have initiated and developed in the previously created but optically undetectable channel.

At the same time, we cannot rule out a possibility that there were no positive leader/streamer branches emanating from the predominantly horizontal channel or bidirectional leaders before BL_1, because (a) leaders in virgin air are known (e.g., Berger and Vogelsanger., 1969; Chen et al., 1999; Lu et al., 2008; Orville and Idone, (1982)) to be able to propagate at speeds of the order of 10^6 m/s and (b) extension speeds for BL_3 and BL_4 in our study are considerably higher than those for BL_1 (see Figure 6).

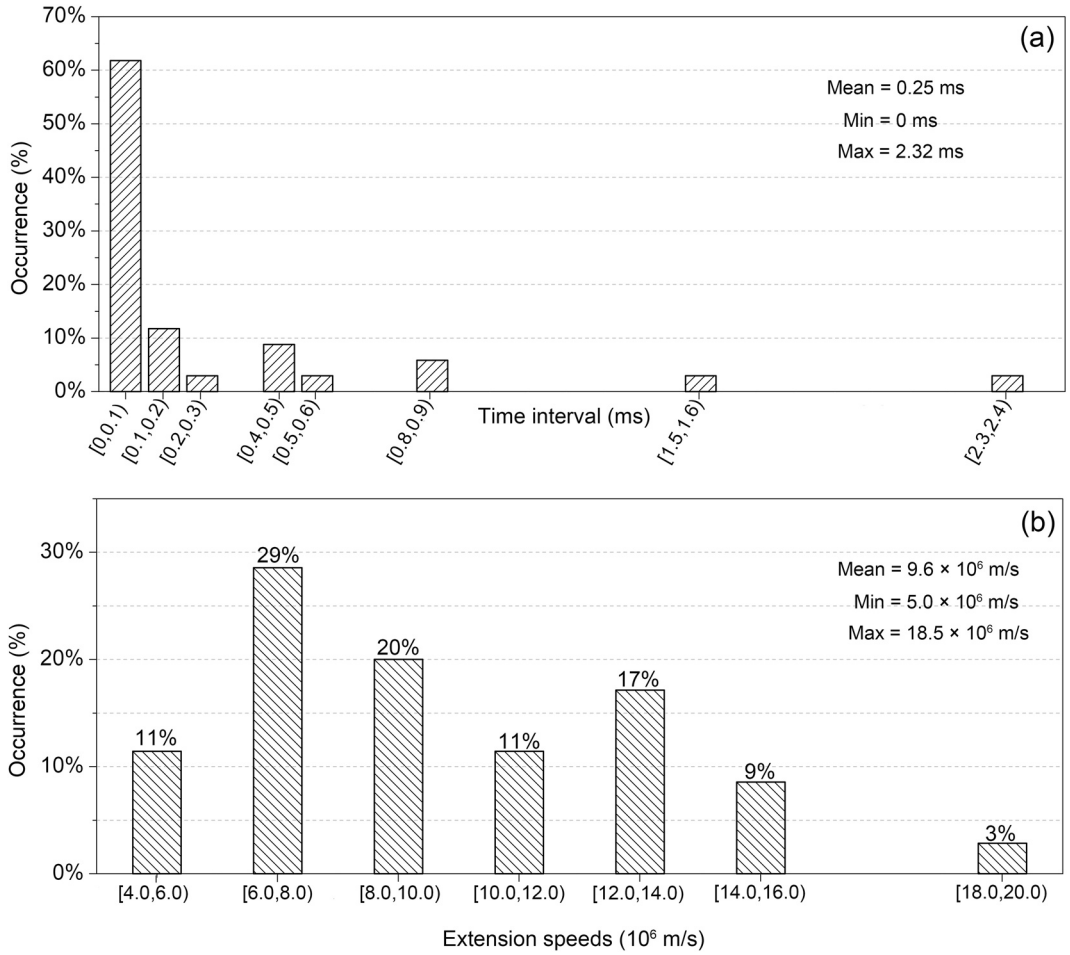

Figure 8. (a) Distribution of time intervals and (b) 2D extension speeds of 36 side branches (see also Table 1).

4.2. Initiation of Vertical Bidirectional Leaders

It is known (e.g., Maslowski and Rakov, 2006) that the bulk of leader charge is contained in the corona (space charge) sheath formed around the narrow hot core. Therefore, the horizontal channel seen in our high-speed video camera images is a narrow hot core surrounded by optically undetectable corona sheath, whose outer radius should be up to tens of meters (e.g., for leader line charge density of 1 mC/m, the corona-sheath radius should be about 20 m, according to Gauss Law). The horizontal channel was positive at the time of BL_1–BL_4. The shielding effect of the positive corona sheath around the positive hot core should suppress the development of branches directly from the core. For this reason, such branches are more likely to be formed via bidirectional leaders excited outside the positive corona sheath. BL_1 to BL_4 initiated at distances of approximatively 250 to 700 m from the luminous horizontal channel, from which we infer that the radius of the positive corona sheath was less than 250 m. It is worth noting that the radius of corona sheath for positive polarity is expected to be greater than that for negative polarity (because of the lower propagation field threshold for positive streamers) and that the initiation point of later BLs should have been influenced by the presence of remnants of preceding BLs.

4.3. Dynamics of Bidirectional Leaders

We start with a brief overview of the literature on bidirectional leaders making connection to positively charged channels. Most of the time, bidirectional leaders are completely or in part hidden inside the cloud, which makes their optical imaging impossible. Therefore, as of today, there are only a few optical observations of bidirectional leaders found in the literature. Montanyà et al. (2015) and Warner et al. (2016)

reported on bidirectional leaders making connection to pre-existing positively charged channels of cloud and ground lightning discharges, respectively. Further, Pilkey (2014, Figures. A-1 and A-2) reported on a floating channel segment that initiated about 84 m from the positive in-cloud leader channel near 3-km altitude and 364 μs later connected to the lateral surface of that channel. Tran and Rakov (2016), using a high-speed video camera, observed a natural lightning discharge that started with a bidirectional leader. The negative end of the bidirectional leader extended toward the ground (and eventually produced a RS), while its positive end, developing primarily horizontally, exhibited an abrupt extension that was relatively straight and had a 2-D length of about 1 km. Tran and Rakov (2016) tentatively interpreted this event as a gigantic, kilometer-scale positive-leader step that developed from a space stem/leader and connected to the lateral surface of the existing positive channel, creating a major positive branch. This newly created branch faded and then was re-illuminated four times with a remarkably constant time interval of 1.2 ms. The rate at which the new positive branch was formed was at least 1.6×10^6 m/s if it originated from the mid-point of the newly formed branch. Additionally, Pu and Cummer (2019), who used a 100–200 MHz broadband interferometer, observed a bidirectional leader that initiated approximately 500 m from a positive in-cloud channel and whose negative end connected to the positive channel.

In this study, the formation of a new downward positive branch was facilitated by four bidirectional leaders sequentially retracing the same path. The resultant downward branch elongated abruptly at the time of negative end of BL_1 and BL_4 connected to the floating horizontal channel (see Figures 4f and 5j). Some elongation of the positive ends of BLs prior to connection could have occurred in the same frame. The lengths of abrupt elongations of new branches were obtained by comparing the tip positions in the connection frame and in the frame immediately after connection (see Figures 4e and 4f; Figures 5i, 5j and 3h). The abrupt extension events exhibited some similarities with the so-called restrike phenomenon reported by Les Renardieres Group (1972, 1977) from long positive laboratory spark experiments. However, the 2-D speeds of the abrupt extensions (BL_1, approximately 1.1×10^7 m/s in virgin air; BL_4, approximately 5.4×10^7 m/s along the remnants of BL_3 and extended into virgin air, unless there was an optically undetectable channel prior to BL_1) were much higher than the long-spark restrike speeds (0.5 to 2.0×10^5 m/s) based on the observations of Chen et al. (2016). The abrupt extension lengths (approximately 530 and 1,070 m) were much larger than the abrupt extensions of the positive end of a subsequent leader (approximately 91–160 m) reported by Wu, Lyu, Qi, Ma, Chen, Jiang et al., (2019), but were comparable to that of the 1-km-long extension occurring at the positive end of the bidirectional leader observed by Tran and Rakov (2016).

4.4. Side Branches From the Lateral Surface of the Horizontal Channel in Response to +CG

Before the +CG RS, the vertical and horizontal channels each consisted of a narrow hot core surrounded by an optically undetectable radial corona sheath containing the positive space charge deposited there by the leader. The 135-kA +CG RS effectively transported negative charge toward the junction point and into the horizontal channel, to neutralize the positive leader charge. The negative charge (some tens of coulombs expected for the 135-kA peak current) rapidly injected into the horizontal-channel hot core caused negative breakdown, in the form of side branches, into the positive corona sheath surrounding the hot core. The side branches extended over roughly 110 to 740 m with a mean of 290 m (probably beyond the positive corona sheath, which is expected to have radial dimension up to tens of meters) at speeds ranging from ~0.5 to 1.9×10^7 m/s with a mean of 9.6×10^6 m/s and exhibited flickering. It is likely that the side branches are the most intense (thermalized) streamers of the so-called reverse corona discussed in detail by Maslowski and Rakov (2006, 2009).

In some respects the side branches are similar to the recently discovered "needles" observed via RF channel imaging by Hare et al. (2019) and Pu and Cummer (2019) and optically by Saba et al. (2020). The similarities include (a) the extension from the lateral surface of positively charged channels, (b) lengths of the order of 10–100 m (from 30 to 100 m in Hare et al. (2019), 60 m in Pu and Cummer (2019), and from 2.3 to 73 m (mean = 14.3 m) in Saba et al. (2020); in our case a little longer), and (c) flickering. On the other hand, extension speeds are different: 10^5 to 10^6 m/s for "needles" (3×10^5 m/s in Hare et al. (2019), 1–10×10^5 m/s in Pu and Cummer (2019), and 2.7×10^5 m/s (on average, 2-D) in Saba et al. (2020)) versus 10^6 to 10^7 m/s for our side branches. Also, "needles" flicker at time intervals of some milliseconds (from 3 to 7 ms in Hare et al. (2019), from 6 to 7 ms in Pu and Cummer (2019), and from 0.3 to 34 ms (mean = 2.6 ms) in Saba

et al. (2020)), while our side branches flicker at intervals of a factor of 10 to 100 shorter (mean = 0.1 ms). Thus, our side branches extend faster and flicker at a higher rate. The reason for the difference in the extension speed and flickering rate between our side branches and the "needles" may be that the 135-kA-return-stroke later stage and the following continuing current of our +CG flash injected a considerably large negative charge (tens of coulombs are expected) into the positive horizontal channel than charges associated with in-cloud positive leaders studied by Hare et al. (2019) and Pu and Cummer (2019) or upward positive leaders developing from grounded objects reported by Saba et al. (2020). Positive leader currents in upward and rocket-and-wire triggered lightning are of the order of 100 A (Miki et al. (2005)), about two orders of magnitude lower than continuing currents following RSs in +CG flashes (Rakov and Uman, 2003, p.222). Of course, the two phenomena occur in different contexts (leader vs. RS), but their physics should be similar. In our future work, we will quantify the characteristics of side branches in more detail and compare more parameters of streamer-like filaments observed in this study (see also Wu et al. (2020) published in ESSOAR) and needle-like structures reported by Hare et al. (2019), Pu and Cummer (2019), and Saba et al. (2020).

Data Availability Statement

This study complies with the AGU data policy. All the lightning data supporting the conclusion of the paper are available online (https://figshare.com/s/935f069050a8d9a8cadb).

Acknowledgments
This work was supported in part by the National Key R&D Program of China (Grant 2017YFC1501504), the National Natural Science Foundation of China (Grant 41805005 and 41775010), and in part by the National Science Foundation (Grant AGS-1701484).

References

Berger, K., & Vogelsanger, E. (1969). New results of lightning observations. In S. C. Coroniti, & J. Hughes (Eds.), *Planetary electrodynamics* (pp. 489–510). New York. Gordon and Breach.

Chen, M., Takagi, N., Watanabe, T., Wang, D., Kawasaki, Z., & Liu, X. (1999). Spatial and temporal properties of optical radiation produced by stepped leaders. *Journal of Geophysical Research*, *104*, 27573–27584. https://doi.org/10.1029/1999jd900846

Chen, S., Zeng, R., Zhuang, C., Zhou, X., & Ding, Y. (2016). Experimental study on branch and diffuse type of streamers in leader restrike of long air gap discharge. *Plasma Science and Technology*, *18*, 305–310. https://doi.org/10.1088/1009-0630/18/3/15

Hare, B. M., Scholten, O., Dwyer, J., Trinh, T. N. G., Buitink, S., ter Veen, S., et al. (2019). Needlelike structures discovered on positively charged lightning branches. *Nature*, *568*(7752), 360–363. https://doi.org/10.1038/s41586-019-1086-6

Jiang, R., Wu, Z., Qie, X., Wang, D., & Liu, M. (2014). High-speed video evidence of a dart leader with bidirectional development. *Geophysical Research Letters*, *41*, 5246–5250. https://doi.org/10.1002/2014GL060585

Kong, X., Qie, X., & Zhao, Y. (2008). Characteristics of downward leader in a positive cloud-to-ground lightning flash observed by high-speed video camera and electric field changes. *Geophysical Research Letters*, *35*, L05816. https://doi.org/10.1029/2007gl032764

Kostinskiy, A. Y., Syssoev, V. S., Bogatov, N. A., Mareev, E. A., Andreev, M. G., Makalsky, L. M., et al. (2015). Infrared images of bidirectional leaders produced by the cloud of charged water droplets. *Journal of Geophysical Research: Atmospheres*, *120*, 10728–10735. https://doi.org/10.1002/2015jd023827

Les Renardieres Group. (1972). Research on long air gap discharges at Les Renardieres. *Electra*, *23*, 53–157.

Les Renardieres Group. (1977). Positive discharges in long air gaps at Les Renardieres, 1975 results and conclusions. *Electra*, *53*, 31–153.

Lu, W., Chen, L., Ma, Y., Rakov, V. A., Gao, Y., Zhang, Y., et al. (2013). Lightning attachment process involving connection of the downward negative leader to the lateral surface of the upward connecting leader. *Geophysical Research Letters*, *40*, 5531–5535. https://doi.org/10.1002/2013gl058060

Lu, W., Chen, L., Zhang, Y., Ma, Y., Gao, Y., Yin, Q., et al. (2012). Characteristics of unconnected upward leaders initiated from tall structures observed in Guangzhou. *Journal of Geophysical Research*, *117*, D19211. https://doi.org/10.1029/2012jd018035

Lu, W., Wang, D., Takagi, N., Rakov, V., Uman, M., & Miki, M. (2008). Characteristics of the optical pulses associated with a downward branched stepped leader. *Journal of Geophysical Research*, *113*, D21206. https://doi.org/10.1029/2008jd010231

Maslowski, G., & Rakov, V. A. (2006). A study of the lightning channel corona sheath. *Journal of Geophysical Research*, *111*(D14). https://doi.org/10.1029/2005JD006858

Maslowski, G., & Rakov, V. A. (2009). New insights into lightning return-stroke models with specified longitudinal current distribution. *IEEE Transactions on Electromagnetic Compatibility*, *51*(3), 471–478. https://doi.org/10.1109/temc.2009.2017200

Miki, M., Rakov, V. A., Shindo, T., Diendorfer, G., Mair, M., Heidler, F., et al. (2005). Initial stage in lightning initiated from tall objects and in rocket-triggered lightning. *Journal of Geophysical Research*, *110*, D02109. https://doi.org/10.1029/2003jd004474

Montanyà, J., van der Velde, O., & Williams, E. R. (2015). The start of lightning: Evidence of bidirectional lightning initiation. *Scientific Reports*, *5*, 15180. https://doi.org/10.1038/srep15180

Nag, A., & Rakov, V. A. (2012). Positive lightning: An overview, new observations, and inferences. *Journal of Geophysical Research*, *117*(D8). https://doi.org/10.1029/2012JD017545

Orville, R. E., & Idone, V. P. (1982). Lightning leader characteristics in the Thunderstorm Research International Program (TRIP). *Journal of Geophysical Research*, *87*, 11177–11192. https://doi.org/10.1029/jc087ic13p11177

Pilkey, J. T. (2014). The physics of lightning studied using lightning mapping array, electric field, and optical measurements, PhD dissertation, University of Florida.

Pu, Y., & Cummer, S. A. (2019). Needles and lightning leader dynamics imaged with 100–200 MHz broadband VHF interferometry. *Geophysical Research Letters*, *46*(22), 13556–13563. https://doi.org/10.1029/2019gl085635

Qi, Q., Lyu, W., Wu, B., Ma, Y., Chen, L., & Liu, H. (2018). Three-dimensional optical observations of an upward lightning triggered by positive cloud-to-ground lightning. *Atmospheric Research*, *214*, 275–283. https://doi.org/10.1016/j.atmosres.2018.08.003

Rakov, V. A., & Uman, M. A. (2003). *Lightning: Physics and effects*. New York. Cambridge University Press.
Saba, M. M. F., Campos, L. Z. S., Krider, E. P., & Pinto, O., Jr. (2009). High-speed video observations of positive ground flashes produced by intracloud lightning. *Geophysical Research Letters*, *36*, L12811. https://doi.org/10.1029/2009gl038791
Saba, M. M. F., Cummins, K. L., Warner, T. A., Krider, E. P., Campos, L. Z. S., Ballarotti, M. G., et al. (2008). Positive leader characteristics from high-speed video observations. *Geophysical Research Letters*, *35*, L07802. https://doi.org/10.1029/2007gl033000
Saba, M. M. F., Paiva, A. R. D., Concollato, L. C., Warner, T. A., & Schumann, C. (2020). Optical observation of needles in upward lightning flashes. *Scientific Reports*, *10*, 41598. https://doi.org/10.1038/s41598-020-74597-6
Shao, X., Rhodes, C. T., & Holden, D. N. (1999). RF radiation observations of positive cloud-to-ground flashes. *Journal of Geophysical Research*, *104*(D8), 9601–9608. https://doi.org/10.1029/1999jd900036
Takamatsu, K., Takagi, N., & Wang, D. (2015). Characteristics of the brief but bright discharges that often occur along the trails of positive leaders. *Journal of Atmospheric Electricity*, *35*, 17–30. https://doi.org/10.1541/jae.35.17
Tran, M. D., & Rakov, V. A. (2016). Initiation and propagation of cloud-to-ground lightning observed with a high-speed video camera. *Scientific Reports*, *6*, 39521. https://doi.org/10.1038/srep39521
Wang, D., Watanabe, T., & Takagi, N. (2011). A high speed optical imaging system for studying lightning attachment process. 7th Asia-Pacific International Conference on Lightning. https://doi.org/10.1109/apl.2011.6111050
Warner, T. A., Saba, M. M. F., Schumann, C., Helsdon, J. H., & Orville, R. E. (2016). Observations of bidirectional lightning leader initiation and development near positive leader channels. *Journal of Geophysical Research: Atmospheres*, *121*, 9251–9260. https://doi.org/10.1002/2016jd025365
Wu, B., Lyu, W., Qi, Q., Ma, Y., Chen, L., Jiang, R., et al. (2019). High-speed video observations of recoil leaders producing and not producing return strokes in a Canton-Tower upward flash. *Geophysical Research Letters*, *46*, 8546–8553. https://doi.org/10.1029/2019gl083862
Wu, B., Lyu, W., Qi, Q., Ma, Y., Chen, L., Jiang, R., et al. (2020). A +CG flash caused by a sequence of bidirectional leaders that served to form a ground-reaching branch of a pre-existing horizontal channel. Preprint published in ESSOAR on Aug 11. https://doi.org/10.1002/essoar.10503631.1
Wu, B., Lyu, W., Qi, Q., Ma, Y., Chen, L., Zhang, Y., et al. (2019). Synchronized two-station optical and electric field observations of multiple upward lightning flashes triggered by a 310 kA +CG flash. *Journal of Geophysical Research: Atmospheres*, *124*, 1050–1063. https://doi.org/10.1029/2018JD02937
Yuan, S., Jiang, R., Qie, X., Sun, Z., Wang, D., & Srivastava, A. (2019). Development of side bidirectional leader and its effect on channel branching of the progressing positive leader of lightning. *Geophysical Research Letters*, *46*, 1746–1753. http://doi.org/10.1029/2018GL080718